Subsonic Aerodynamics of Rectangular Parallelepiped Shapes of Fineness Ratio of One-Half

E. F. Lucero* and J. C. Hagan†
Johns Hopkins University, Laurel, Maryland
and
Martin E. Beyers‡
National Research Council of Canada, Ottawa, Canada

Results from static and dynamic stability wind-tunnel tests at subsonic speeds are presented for rectangular cylinders having a fineness ratio of about one-half. Aerodynamic data were obtained over ranges of angles of attack and roll sufficient to construct aerodynamic inputs to a six-degree-of-freedom re-entry simulation for the full rotational motion experienced by a free-falling body. The effects of Reynolds number, edge roundness, angle of attack, and roll angle were investigated. Free-fall tests of the model are also described. The aerodynamic characteristics were found to be highly nonlinear with the various geometric and flow variables investigated, especially at attitudes near broad face and narrow side to the wind.

Nomenclature

(See Figs. 3 and 4 for definitions, magnitudes, and directions of forces and angles. Angles are in radians unless otherwise noted.)

C_A = axial force coefficient, ≡axial force (lb)/$\bar{q}S$
C_ℓ = rolling moment coefficient, ≡rolling moment (ft-lb)/$\bar{q}SL$
C_m = pitching moment coefficient, ≡pitching moment (ft-lb)/$\bar{q}SL$ referenced to the model centroid
C_N = normal force coefficient, ≡normal force (lb)/$\bar{q}S$
C_n = yawing moment coefficient, ≡yawing moment (ft-lb)/$\bar{q}SL$ referenced to the model centroid
$C_{\ell_p}^*$ = roll damping coefficient, 1/rad
$= C_{\ell_p} + C_{\ell_{\dot\beta}} \sin\alpha - C_{\ell_{\dot\alpha}} \cos\alpha \tan\beta$
C_{ℓ_j} $= \partial C_\ell / [\partial(jL/2V)]$, $j = p, \dot\alpha, \dot\beta$; $p \equiv \dot\phi$
$C_{m_q}^*$ = pitch damping coefficient, $= C_{m_q} + C_{m_{\dot\alpha}}$ 1/rad
C_{m_j} $= \partial C_m / \partial(jL/2V)$, $j = q, \dot\alpha$; $q \equiv \dot\theta$
$C_{n_r}^*$ = yaw damping coefficient, $= C_{n_r} + C_{n_\beta} \cos\alpha$, 1/rad
C_{n_j} $= \partial C_n / [\partial(jL/2V)]$, $j = r$; $\dot\beta$; $r \equiv \dot\psi$
c = streamwise length of two-dimensional shapes at $\alpha = 0$ deg (see Fig. 5)
h = length of model along the Z_m axis, ft
l = length of model along the X_m axis, ft
l_s = length of sting, ft
L = length of model along the Y_m axis, ft
M = Mach number
p,q,r = roll, pitch, and yaw angular rates, rad/s
$\bar{q}$ = dynamic pressure, lb/ft^2
R = corner radius, ft
Re_h = Reynolds number based on length h
S = reference area Lh, ft^2
V = velocity, ft/s
X,Y,Z = axis system defined in Figs. 3 and 4
X_{cp} = center-of-pressure location along the X axis; positive aft of leading edge, ft
α_R = resultant angle of attack, angle between the velocity vector and X axis of model, rad
α = angle of attack in the X-Z plane, rad
β = angle of sideslip, $\beta = -\psi$, rad
ϕ,ψ,θ = roll, yaw, and pitch angles, rad
ν = kinematic viscosity, ft^2/s

Subscripts

m = model
T = tunnel
term = terminal velocity conditions

Received Dec. 23, 1985; presented as Paper 86-0399 at the AIAA 24th Aerospace Sciences Meeting, Reno, NV, Jan. 6-9,1986; revision received Aug. 29, 1986.

*Engineer, Fluid Dynamics Group, Applied Physics Laboratory. Member AIAA.
†Program Manager, Aerospace Nuclear Safety Program, Applied Physics Laboratory. Member AIAA.
‡Senior Research Officer, Unsteady Aerodynamics Laboratory. Member AIAA.

Introduction

THE General-Purpose Heat Source (GPHS) module (Fig. 1) is one of a number of similar rectangular parallelepiped containers that house the radioactive materials that will be used to provide electricity for the Galileo mission to Jupiter and the Solar Polar (Ulysses) flight out of the ecliptic. The Galileo mission requires 36 of these modules and the Ulysses mission 18. An extensive safety analysis and risk evaluation precedes any mission that carries nuclear materials.[1] One aspect of this risk evaluation considers the consequences of re-entry following a launch failure. The GPHS modules are designed to survive re-entry and subsequent impact on Earth. Structural impact tests using flight hardware are conducted to evaluate the impact performance of the module. Preliminary tests at the Los Alamos National Laboratory have indicated that the structural response is sensitive to the attitude of the module at the time of impact. To gain the most data from the limited number of available test articles, it is useful to know the most probable orientation of the module at the time of impact.

To aid in the determination of impact attitudes, six-degree-of-freedom (6DOF) digital simulations of the re-entry of a module are being conducted. Since the module motion prior to impact is dependent on the aerodynamic characteristics at flow conditions near terminal speeds, this flow regime has been addressed intensively in the aerodynamic experimental investigations. The terminal velocity of the GPHS module was determined from helicopter drop tests. It averaged 165 ft/s, which corresponds to an average drag coefficient of 1.01 and a Reynolds number of $Re_h \approx 0.3 \times 10^6$ from sea level to 5000 ft.

Earlier aerodynamic tests at hypersonic speeds indicated that a model without chamfers could trim with the narrow side leading, which was considered structurally undesirable. The chamfers on the baseline configuration (Fig. 1) were therefore incorporated to assure that the configuration was unstable with the narrow side to the wind, i.e., at $\alpha = 90$ deg.

The general objective of these investigations was to determine the impact angle of the GPHS module if it should reenter the Earth's atmosphere. The primary objective of the subsonic wind-tunnel tests was, therefore, to obtain six-component aerodynamics on the GPHS module that could be used to generate inputs to the JHU/APL 6DOF re-entry program. Secondary objectives were to investigate the effects of Reynolds number, edge roundness, and leading-edge chamfers.

Description of Tests

Three distinct wind-tunnel tests were conducted[2-4] to obtain aerodynamic static and dynamic stability and axial force data on the GPHS module configuration (Fig. 1); perturbations therefrom were represented by a series of models without chamfers (Fig. 2). The axis system adopted for the aerodynamic studies is given in Figs. 3 and 4. The rationale for the tests, test models, instrumentation, test conditions, and procedures are described in this section. The results of the tests are described in a subsequent section.

Free-Flight Tests

The free flights were conducted in the vertical tunnel of the Air Force Wright Aeronautical Laboratories (AFWAL).[2] The primary objective of the tests was to obtain qualitative information on the motion of the GPHS module at terminal speeds, specifically to determine if the module had a preferred trim angle of attack.

Two sets of models of three each were designed for levitation in the AFWAL vertical tunnel using a design drag coefficient of $C_D = 1.01$, determined from previous helicopter drop tests. One set simulated the actual values of moments of inertia of the GPHS module, but had different masses and scales; the other set had a scale of 1.0, but had different masses and moments of inertia. The design variables were influenced by test results obtained by Bustamante and Stone,[5] which showed that autorotational rates were influenced by the model size but not by the moment of inertia about the spin axis.

The test procedure involved hand-placing each model repetitively in the freestream with and without spin and adjusting the speed of the tunnel until the model levitated for a reasonable amount of time. The preferred motions along with the terminal speeds (and hence the drag) of the models were deduced from visual observation, movie film, and video tape.

Static Stability Tests

The static stability and axial force tests were conducted at the Vought Corporation low-speed tunnel. Both aft-mounted (along the X_m axis) and side-mounted (along the Y_m axis) models (Figs. 3 and 4) were tested in the range of tunnel angle of attack, $\alpha_T = -20$ to 90 deg. The data from the side-mounted models were used to extend the range in α_R since the objective was to define the module aerodynamics from $\alpha_R = 0$ to 360 deg.

The effect of Reynolds number was investigated in the range permitted by the tunnel operating conditions, $Re_h = 3.34 \times 10^5$ to 9.15×10^5. This investigation was conducted because previous investigations with two-dimensional bodies[6] (models spanning the tunnel sidewalls) showed that the transitional Reynolds number based on streamwise length was about 5×10^5, depending on shape and edge roundness (Figs. 5 and 6). The Reynolds number for the GPHS module at terminal velocity is in this critical region for two-dimensional bodies. The edge roundness for the module is much less than that which generates transition on two-dimensional bodies at the values of Re_h of interest here; however, it was not known how

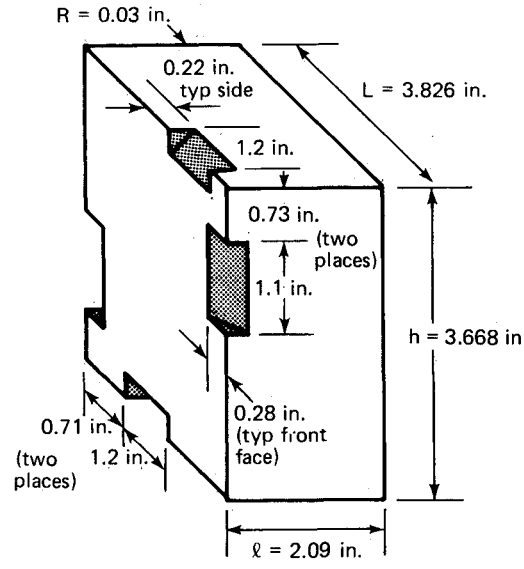

Fig. 1 GPHS module (configuration I, scale = 1.0).

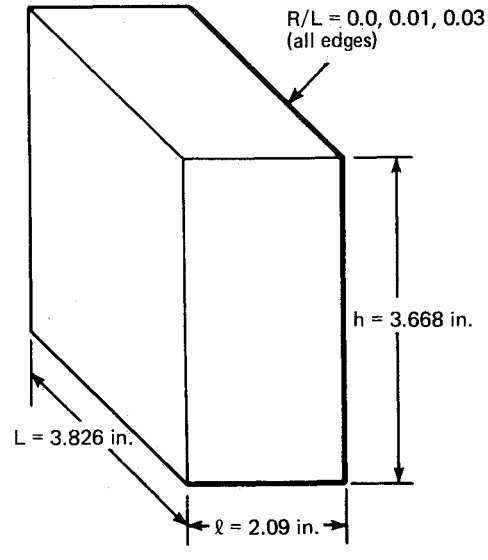

Fig. 2 GPHS module, configuration II (scale = 1.0 wind-tunnel model).

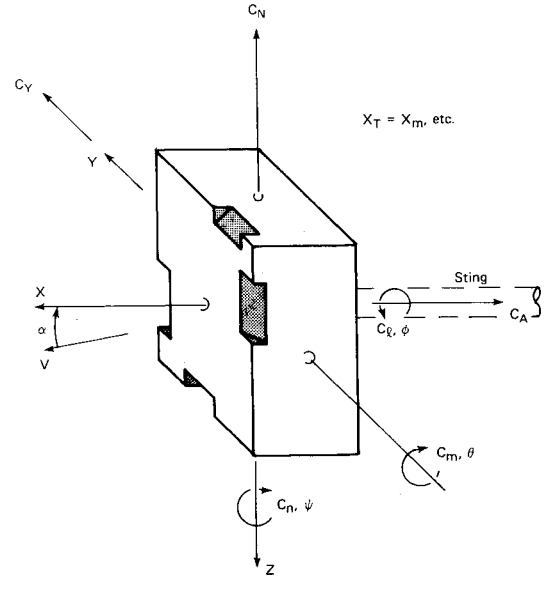

Fig. 3 Model and tunnel axis systems shown at $\psi_m = 0$ deg, $\phi_m = 0$ deg (aft-mounted model).

the three-dimensionality of the body will affect the sensitivity to transition, although it was expected that it will decrease it. For this reason and because ablation during re-entry can increase the edge roundness, models were constructed to check the effect of R/L (Fig. 2).

Some aerodynamic static force and moment data on two-dimensional models and on missile bodies with rectangular cross sections have been published,[6–10] but aerodynamic data on parallelepipeds (three-dimensional shapes) of low fineness ratio were very sparse. Virtually, the only aerodynamic test data available on rectangular parallelepipeds of low fineness ratio prior to this test were those obtained by W. Maguire, K. Phillips, E. O'Neill, and others at the David Taylor Naval Ship Research and Development Center (DTNSRDC) transonic wind tunnel.[11] These data, shown in Fig. 7, were obtained mostly at $M \geq 0.60$ and the configurations were of fineness ratio equal to or greater than 1.0. These results were used for guidance in estimating the subsonic aerodynamics for the GPHS module and for correlations with the present test results.

Forced Oscillation Tests

The roll damping and pitch damping tests were conducted in the National Research Council/Canada, 2×3 m low-speed wind tunnel.[4] The configurational and flow variables were basically the same as for the static stability tests, except that the models were designed by NRC to be compatible with existing or developed test apparatus and to meet the requirements for equivalent oscillation frequencies in pitch and roll and minimum dynamic sting interference. While the roll damping tests could be performed on an existing NRC apparatus, a new pitch damping apparatus had to be developed for use with these very short, blunt configurations at low speeds. In both cases, the apparatus is electromechanically driven and a servo system provides the necessary control to maintain an amplitude-stabilized motion at the resonance frequency of the mechanism.

The measurement technique used[4,12] was common to both the pitch and roll apparatuses. Cross correlations between the primary motion and drive torque signals were performed in analog form. A direct-tare procedure was used to eliminate the nonaerodynamic loads. The aerodynamic derivatives were obtained from measurements of the in-phase and quadrature components of the drive torque and from the frequency of oscillation. The data reduction technique is described in Ref. 4.

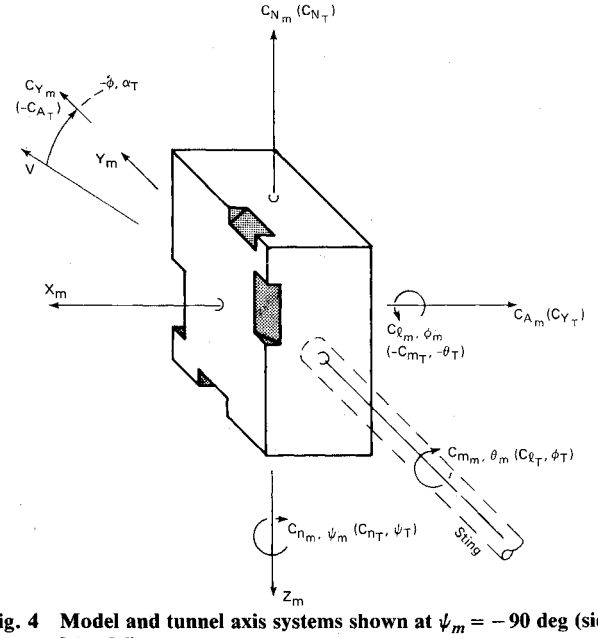

Fig. 4 Model and tunnel axis systems shown at $\psi_m = -90$ deg (side-mounted model).

The nominal reduced frequency was 0.22 and the nominal oscillation amplitudes in pitch, yaw, and roll were ±1.5 deg.

The correct functioning of the dynamic measurement system was verified following standard procedures. The dynamic calibrator simulated the oscillatory aerodynamic forces on the model by generating known loads at the test frequency. Thus, the overall verification of the complete system, including the apparatus instrumentation and data acquisition system, is accomplished when the input loads were correctly determined.

The dynamic stability of two-dimensional rectangular cylinders has been extensively researched,[13-16] but few descriptions of the stability of three-dimensional rectangular parallelepipeds have appeared in the open literature. Investigations conducted by O'Neill et al.[11] on pitch damping were the most extensive (Fig.8). These provided some guidance in making the initial estimates of $C_{m_q}^*$ for the GPHS.

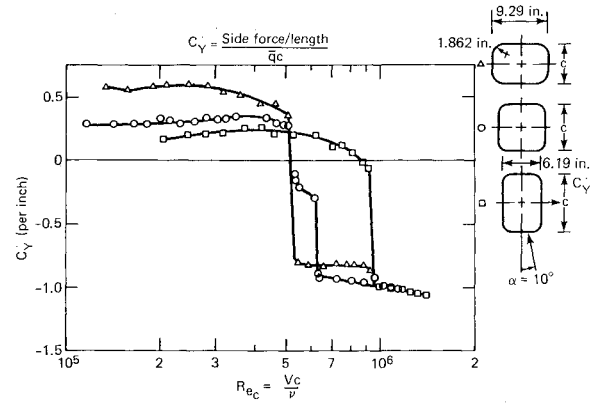

Fig. 5 Effect of aspect ratio and *Re* on C_Y (Ref. 6).

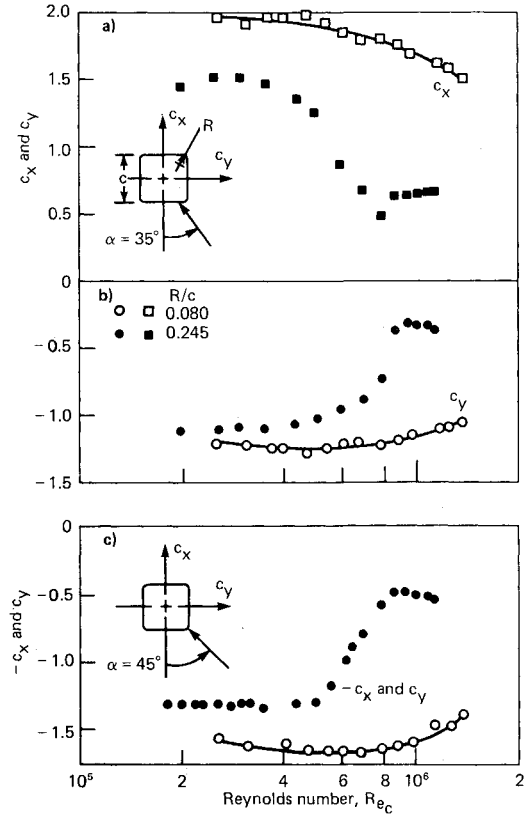

Fig. 6 Effect of edge roundness on section axial and side force coefficients, two-dimensional cylinders (from Figs. 4d and 5d, Ref. 6).

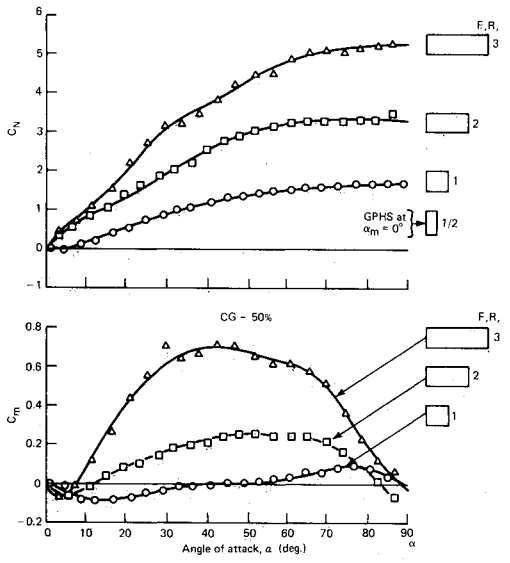

Fig. 7 Effect of fineness ratio on C_N and C_m, $M=0.74$ (from Fig. 4 of Ref. 11).

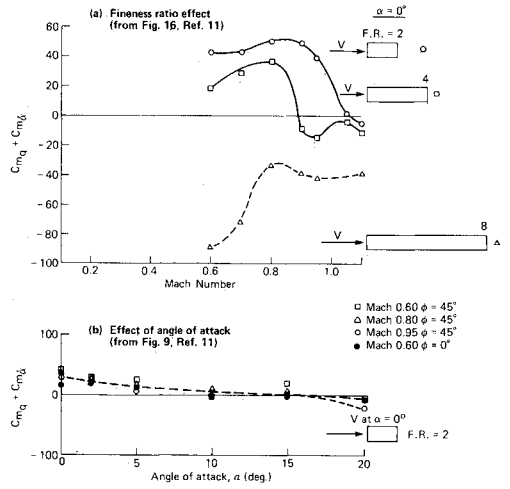

Fig. 8 Effect of various geometric and flow variables on $C_{m_q} + C_{m_{\dot\alpha}}$ (Ref. 11).

Test Results

Free-Flight Test Results

The motion at terminal speeds was deduced from visual observations to be as follows. For the models that simulated the moments of inertia, the models tended to oscillate with amplitudes of 15–30 deg about the axis of minimum moment of inertia (the Y axis) and to assume a roll rate. The drag coefficient at terminal velocity deduced from the rms value of V_{term} computed for all runs where the model was deemed to levitate was $C_D = 0.96$ for oscillations with chamfers windward and $C_D = 1.05$ for oscillations with chamfers leeward. The rms value for all cases gives $C_D = 1.00$, which agreed with the results from the helicopter drop tests. The model pitching frequency was observed to be inversely proportional to the moment of inertia about the Y axis, as might be expected, but was contrary to certain experimental results for flat plates.[5]

Static Stability Test Results

Effect of Reynolds Number

The effect of Reynolds number on the aerodynamics of the aft-mounted GPHS models was found to be small (Fig. 9). This was also true for the side-mounted models and for the

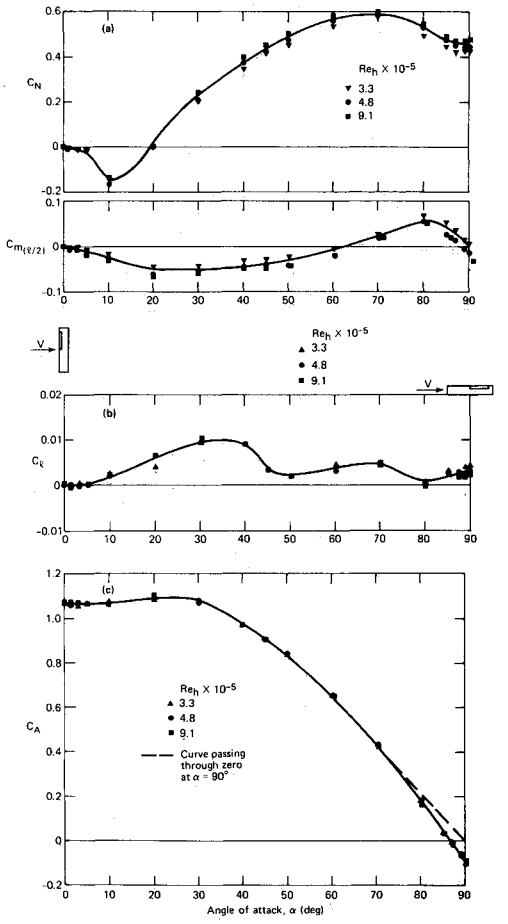

Fig. 9 Effect of Reynolds number on static forces and moments, $\phi = 0$ deg.

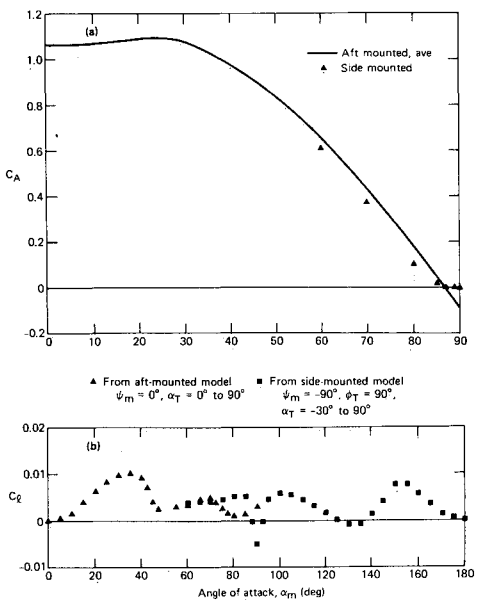

Fig. 10 Comparison of C_A and C_ℓ for aft- and side-mounted models, $\phi_m = 0$ deg.

configurations without chamfers. Except for C_N, a trend with Re_h is not obvious. C_N increases slightly with increasing Re_h at $\alpha \gtrsim 20$ deg. The critical Reynolds number for the configurations tested was not achieved in the range tested.

Effect of Sting Interference

A systematic investigation of the effect of sting and/or support interference on the aerodynamics of blunt bodies of low aspect ratio is not known to exist. A survey of this subject, for both static and dynamic tests, has been published by Ericsson and Reding.[17] A comparison of results from the aft- and side-mounted models provided a measure of the sting interference effects, as well as a basis for extrapolating the measured data to model angles of attack to 360 deg. For example, the aft-mounted model has an induced base pressure when $\alpha_R = 90$ deg, resulting in a negative axial force that is not present on the side-mounted model (Fig. 10a). Similarly, the side-mounted model has an induced pressure on the leeward side at $\alpha_R = 90$ deg that, when acting on the skewed area resulting from the chamfers, produces a net rolling moment at $\alpha_R = 90$ deg which is quite different from that of the aft-mounted model (Fig. 10b).

Effect of Edge Roundness

The effect of edge roundness on C_N, C_A, and C_ℓ is shown in Fig. 11 for the configurations without chamfers. The test data for the GPHS module are also given to show the effect of the chamfers. In general, increasing edge roundness decreases C_A and C_N except that at $\alpha > 60$ deg the opposite trend is present for C_A. Note that at $\alpha < 20$ deg the chamfers have the same effect on C_A and C_N as increasing the edge rounding. The effectiveness of the chamfers in producing a rolling moment is greatest at $10 \lesssim \alpha \lesssim 50$ deg. It will also be shown later that in the region where a pitching moment couple does not exist ($\alpha \gtrsim 20$ deg), increasing edge roundness increases the static stability margin (i.e., X_{cp} moves farther aft of the reference center) at $20 < \alpha \lesssim 50$ deg and decreases it between $\alpha = 80$ and 90 deg.

Effect of Roll Angle

The test results presented in the previous sections were for the models oriented at a roll angle of $\phi = 0$ deg. Sufficient data were also obtained at $\phi \neq 0$ deg to show the importance of roll angle specifically on the aerodynamic parameters that contribute to model rotation in free fall, C_m and C_ℓ (Fig. 12). In all cases, the effect of ϕ is small at $\alpha_R \lesssim 20$ deg and becomes increasingly large as α_R increases. (A positive static stability margin was found to exist for the GPHS module at all roll angles tested when $20 < \alpha_R \lesssim 70$ deg.) The maximum values for C_ℓ occur at $\phi = \pm 22.5$ deg. The effect of ϕ on C_A was small at all values of α_R.

Comparison of C_A with Free-Flight Data

The static force and moment tests verified the qualitative results from free flight. As with free flight, it was found that the axial force coefficient is lower when the chamfers are windward ($\alpha = 0$ deg), than when leeward ($\alpha = 180$ deg). The results from the static tests are $C_A = 1.08$ at $\alpha = 0$ deg and $C_A = 1.2$ at $\alpha = 180$ deg.

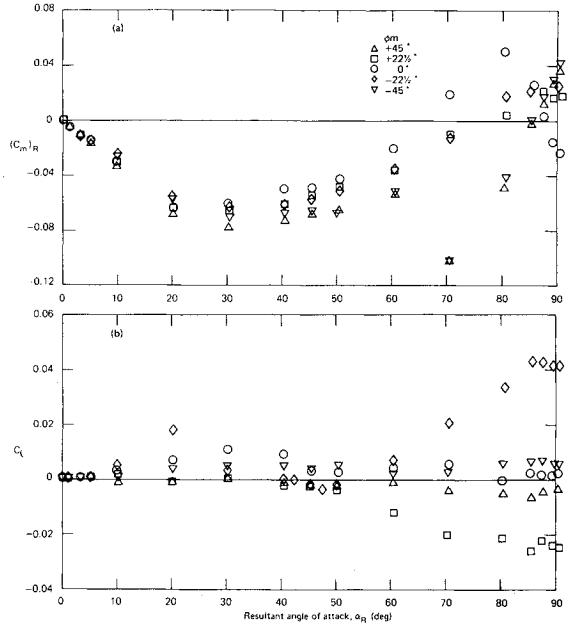

Fig. 12 Effect of roll angle on C_m and C_ℓ, $\phi = 0$ deg.

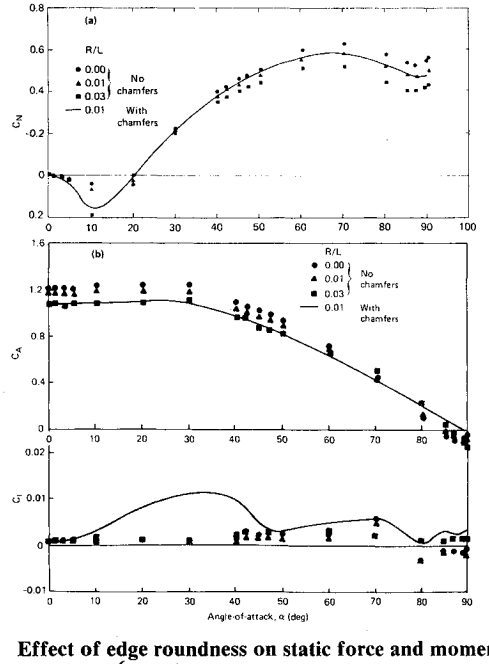

Fig. 11 Effect of edge roundness on static force and moments, $\phi = 0$ deg, $Re_h = 0.68 \times 10^6$.

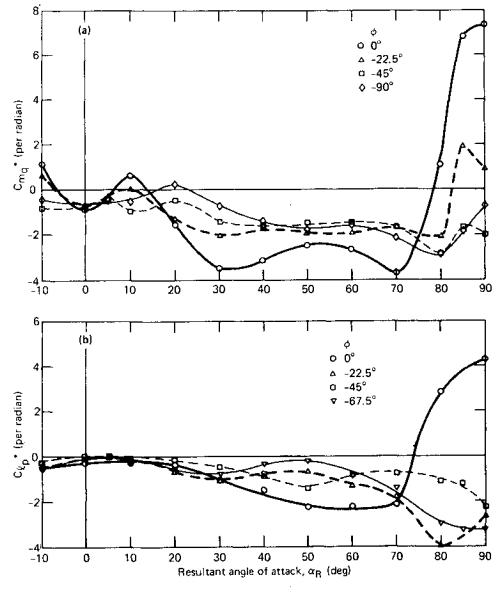

Fig. 13 Effect of roll angle on pitch and roll damping, $Re_h = 0.34 \times 10^6$.

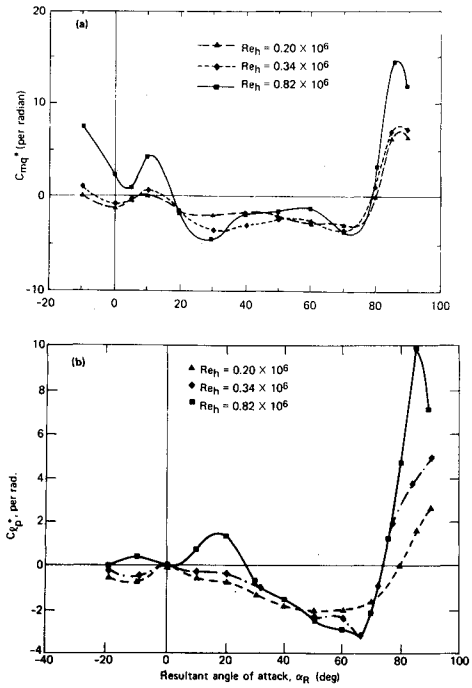

Fig. 14 Effect of Reynolds number on pitch and roll damping, $\phi = 0$ deg.

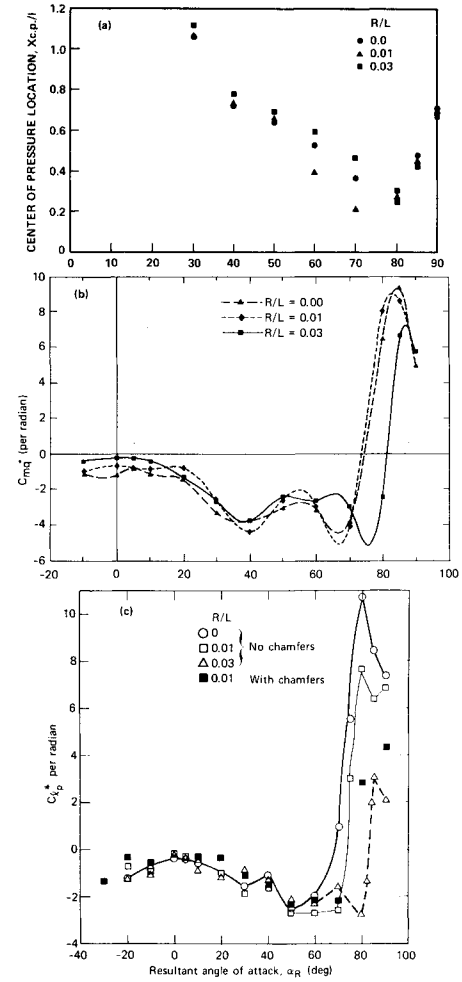

Fig. 15 Effect of edge roundness on center of pressure location and on dynamic stability, $\phi = 0$ deg.

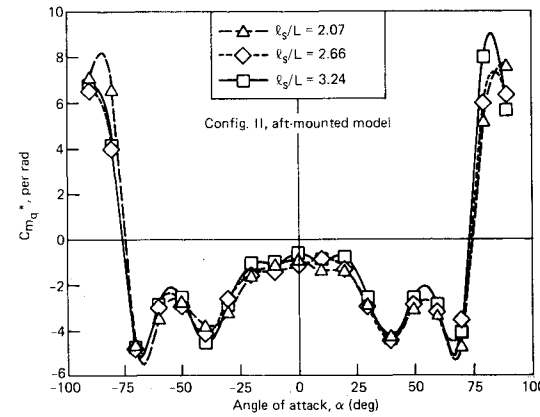

Fig. 16 Effect of sting length on measured C_{mq}^*, $\phi = 0$ deg.

Dynamic Stability Test Results

Effect of Roll Angle

Both C_{mq}^* and $C_{\ell_p}^*$ are strongly dependent on roll angle (Fig. 13). The module is dynamically stable for oscillation in pitch and in roll at most roll angles over the angle-of-attack range $0 \leq \alpha_R \lesssim 80$ deg, but dynamically unstable for small roll angles ($\phi \lesssim |22.5$ deg$|$) at $\alpha \gtrsim 80$ deg (test data are also available at $\phi = 22.5$, 45, and ± 67.5 deg). The destabilizing effect appears to be partly attributable to the unsteady effect arising from the fluctuation of the windward shear layer, which encloses a separation bubble at these attitudes. At $\alpha_R = 90$ deg, the magnitudes of the coefficients are undoubtedly altered by interference from the sting, but the trend with ϕ should remain as shown in Fig. 13.

Effect of Reynolds Number

Whereas the effect of Reynolds number on all static forces and moments was found to be small (e.g., Fig. 9), the effects of Re_h on the pitch and roll damping coefficients, C_{mq}^* and $C_{\ell_p}^*$, were significant (Fig. 14), especially when either the broad face or side face was normal to the wind, $\alpha = 0$ or 90 deg. In the vicinity of $\alpha = 90$ deg, the model was undamped in both pitch and roll at all values of Re_h tested and, in the vicinity of $\alpha = 0$ deg, it was undamped at the highest Re_h tested, $Re_h \approx 8 \times 10^5$. The general trend is one of decreasing dynamic stability with increasing Reynolds number.

Note that, when $Re_h \approx 8 \times 10^5$, large variations with α were obtained in C_{mq}^* and $C_{\ell_p}^*$. No unusual sensitivity of the corresponding static components C_m and C_ℓ were observed in this region of Re_h from the static test results of the GPHS module. However, for the configuration with the largest edge rounding, $R/L = 0.03$, the model in the static tests oscillated at large amplitudes in the region $5 < \alpha < 35$ deg when the Reynolds number was approximately 8×10^5. The difference in sensitivity of the static and dynamic stability to Reynolds number may be related to the effect of motion[18] on the flow separation characteristics. In the presence of oscillatory motion at $Re_h = 8.2 \times 10^5$, it appears that supercritical attached flow behavior was achieved.

Effect of Edge Roundness

The critical edge roundness for two-dimensional bodies as deduced from static stability data was indicated to be much larger than what was tested here.[6] On the other hand, in the dynamic case, the degree of edge roundness could determine whether critical conditions are achieved. An increase in roundness permits the separation point to move aft (and increase the static stability margin, Fig. 15a), thereby limiting the extent of flow separation. Thus, the influence of these separation bubbles on the windward face would be diminished and the

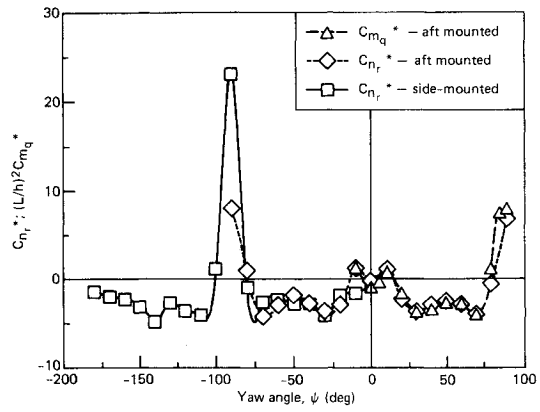

Fig. 17 $C_{n_r}^*$ as a function of $\psi(\phi = 0$ deg).

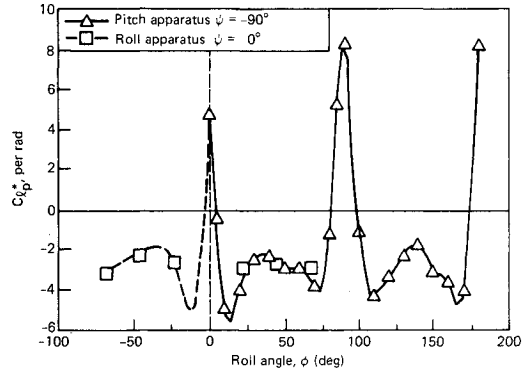

Fig. 18 Effect of measurement systems, $\alpha_R = 90$ deg.

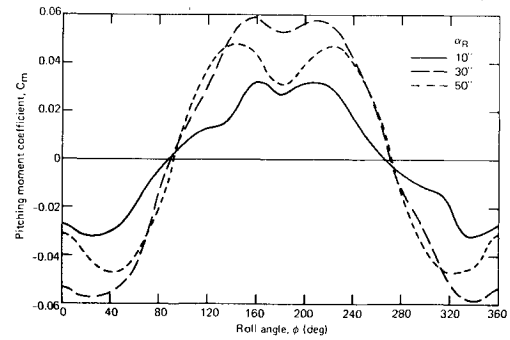

Fig. 19 Construction of pitching moment coefficient with roll angle, subsonic speeds.

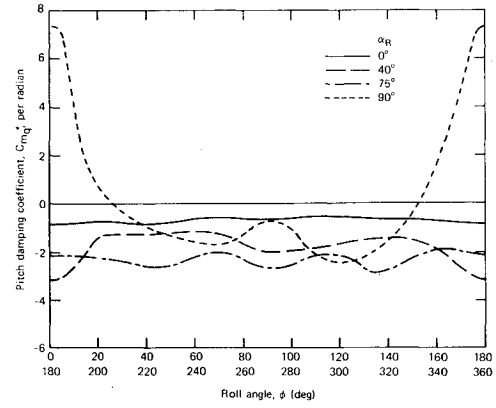

Fig. 20 Construction of pitch damping coefficient with roll angle, subsonic speeds.

dynamic instability decreased. This is evidenced by the effect of R/L on $C_{m_q}^*$ at $\alpha \gtrsim 75$ deg (Fig. 15b). This trend of increasing dynamic stability with increasing edge roundness is more pronounced in the roll damping results (Fig. 15c), as could be expected. This difference in sensitivity of $C_{\ell_p}^*$ and $C_{m_q}^*$ to both Reynolds number and edge roundness may be related to the different directions of oscillation with respect to the velocity vector.[18] For $C_{\ell_p}^*$, the oscillations are transverse to the wind; for $C_{m_q}^*$, the oscillations are generally streamwise. The roundness effects were not significant at $\alpha < 60$ deg.

The chamfers have the same effect on dynamic stability as increased edge roundness (Fig. 15c). The same effect was noted in the static stability results.

Assessment of the Dynamic Stability Results

The measurement uncertainty arising from possible sources of bias error were largely eliminated through extensive calibration and optimization of the data acquisition procedure. The overall magnitude of the remaining effects, including dynamic sting interference, methods of mounting, and sting plunging, was investigated on the basis of complementary dynamic tests where possible.

The effects of sting length on the measurements of pitch damping are small (Fig. 16). The symmetry of the data at small angles for the short sting, $\ell_s/L = 2.07$, suggests that the effect of the strut was also negligible.

The influence of the sting was further explored by studying the effects of the two different methods of mounting. Good agreement was obtained between the yaw oscillation derivatives measured on the aft- and side-mounted models in the range $-80 < \psi < 10$ deg (Fig. 17); however, a large discrepancy appeared in the levels of undamping at $\alpha_R = \psi = -90$ deg. The larger undamping for the side-mounted configuration at this attitude is to be expected, since the sting is then hidden behind the model and cannot interfere with the development of a fluctuating pressure differential over the front and rear faces, as it does in the aft-mounted configuration. In general, for these blunt models, it may be concluded that pitch oscillation results obtained at attitudes placing the sting on the lee side of the model would be more accurate and that dynamic sting interference could be significant when the sting is normal or nearly normal to the flow.

The overall effects that might be introduced by the measurement system were examined by determining the roll damping at common test conditions on two different apparatuses and using different test installations. Results obtained on an aft-mounted model are compared with those from a side-mounted model oscillated in roll on the pitch apparatus (Fig. 18). Excellent agreement is obtained over the common range $0 \leq \phi \leq 90$ deg, providing confidence in the different measurement systems.

The effects of sting plunging on the measured pitch oscillation derivatives, estimated on the basis of a technique relating them to the shift in the axis of rotation,[19] were fairly small, but since the direct force derivatives were not measured, $C_{m_q}^*$ and C_{n_r} could not be corrected for sting plunging effects. The overall accuracy of the damping data determined in all three modes—pitch, yaw, and roll—excluding the plunging effect on the former two was estimated to be ±6% of the respective maximum values of all conditions except in the regions of severe nonlinearity, where the uncertainty could be up to ±13% of the maximum values.

Extrapolation of Test Data—Inputs to 6DOF Simulation

Physical symmetry, the orthogonal relationship of the coefficients (as in yaw damping and pitch damping, Fig. 17), and the complementary set of data derived from side-mounted models are being used to generate the aerodynamic coefficients for $\alpha_R = 0$–360 deg and $\phi = 0$–360 deg. These will be the

inputs to the 6DOF re-entry simulation that is being used to investigate the impact angle of the GPHS module. Examples of this construction are given in Figs. 19 and 20. In this construction, the effects of chamfers when on the lee side are ignored for the $\phi \neq 0$ deg cases, since data are generally not available for $\alpha_R > |90 \text{ deg}|$ when $\phi \neq 0$ deg.

Simulations using successive refinements in the aerodynamic inputs (including estimates, test data at $\phi = 0$ deg, and test values with the magnitudes averaged for ϕ effects) have shown an important sensitivity of the module motion to the levels of both the static and dynamic stability. Simulations that make use of the complete description of the aerodynamics are being developed.

Conclusions

Subsonic static and dynamic stability and axial force data (including free-flight data) have been obtained on the GPHS module over a range of angles of attack and roll orientations spanning at least 90 deg. These data provide the basis for the construction of the aerodynamic inputs to a six-degree-of-freedom re-entry simulation in the full rotational range experienced by a free-falling body. The aerodynamic characteristics are highly nonlinear with angle of attack and roll angle. The effects of roll angle are largest on rolling and pitching moment coefficients and on roll and pitch damping coefficients.

The effects of Reynolds number, edge roundness, and method of mounting (aft or side) are also shown. Essentially, all flow and geometric parameters have some influence on static and dynamic stability, especially at angles of attack α_R near 90 deg (small face to the wind).

The effect of Reynolds number on static stability is small, but the effect is significant on dynamic stability for the ranges in Re_h tested. Edge roundness also has a larger influence on dynamic stability especially near $\alpha_R \lesssim 90$ deg. Edge roundness tends to increase the static stability margin at $\alpha_R \lesssim 50$ deg and both roll and pitch damping at the higher values of α_R ($\alpha_R \gtrsim 70$ deg). The presence of the sting can have a large influence on static and dynamic stability parameters when it is windward.

Acknowledgment

This work was supported by the U. S. Department of Energy, Dr. Gary L. Bennett, Deputy Director, Division of Special Applications.

References

[1]Bennett, G. L., "Overview of the U. S. Flight Safety Process for Space Nuclear Power," *Nuclear Safety,* Vol. 22, No. 4, July-Aug. 1981, pp. 423-434.

[2]Baker, W. M. II, "APL/JHU Free Flight Tests of the General Purpose Heat Source Module," AFWAL, March 1984.

[3]Oldenbuttel, R. H., "A Low Speed Wind Tunnel Test for JHU/APL to Obtain Force and Moment Data on a General Purpose Heat Source Module," Vought Corp., Dallas, TX, LSWT 660, June 1984.

[4]Beyers, M. E. and Kapoor, K. B., "Dynamic Stability Tests of the GPHS Module and a Series of Rectangular Prismatic Configurations at Low Speeds," National Research Council/Canada, Ottawa, Rept. LTR-UA-81, June 1985.

[5]Bustamante, A. C. and Stone, G. W., "The Autorotational Characteristics of Various Shapes in Subsonic and Hypersonic Flows," Sandia Laboratory, Albuquerque, NM, Rept. SC-RR-69-115, April 1969.

[6]Polhamus, E. C., "Effect of Flow Incidence and Reynolds Number on Low-Speed Aerodynamic Characteristics of Several Non-Circular Cylinders with Applications to Directional Stability and Spinning," NASA TR R-29, 1959.

[7]Hoerner, S. F., *Fluid Dynamic Drag,* published by the author, Brick Town, NJ, 1958, Chap. 3.

[8]Bearman, P. W. and Trueman, D. M., "An Investigation of the Flow around Rectangular Cylinders," *Aeronautical Quarterly,* Aug. 1972, pp. 229-237.

[9]Robertson, J. M., Cermak, J. E., and Nayak, S. K., "A Reynolds-Number Effect in Flow Past Prismatic Bodies," *Mechanics Research Communications,* Pergamon Press, New York, Vol. 2, No. 5-6, 1975, pp 279-282.

[10]Daniel, D. C., Yechout, T. R., and Zollars, G. J., "Experimental Aerodynamic Characteristics of Missiles with Square Cross Sections," *Journal of Spacecraft and Rockets,* Vol. 19, March-April 1982, pp. 167-172.

[11]O'Neill, E. B., "A Summary of Some Experimental Aerodynamic Investigations of Blunt Non-Circular Cross Section Bodies," NSRDC Tech. Note AL-156, Feb. 1970.

[12]Hanff, E. S., "Direct Forced-Oscillation Techniques for the Determination of Stability Derivatives in Wind Tunnels," AGARD-LS-114, May 1981, Paper 4.

[13]Nakamura, Y. and Mizota, T., "Torsional Flutter of Rectangular Prisms," *Journal of the Engineering Mechanics Division, American Society of Civil Engineers,* Vol. 101, No. EM2, April 1975, pp. 125-143.

[14]Ericsson, L. E., "Hydroelastic Effects of Separated Flow," *AIAA Journal,* Vol. 21, March 1983, pp. 452-458.

[15]Orlik-Ruckemann, K. G. and La Berge, J. G., "Dynamic Wind Tunnel Tests of the Simulated Shuttle External Cable Trays," *Journal of Spacecraft and Rockets,* Vol. 20, Jan.-Feb. 1983, pp. 5-10.

[16]Parkinson, G. V. and Brooks, N. P. H., "On the Aeroplastic Instability of Bluff Cylinders," *Transactions of the ASME, Journal of Applied Mechanics,* June 1961, pp. 252-258.

[17] Ericsson, L. E. and Reding, J. P., "Review of Support Interference in Dynamic Tests," *AIAA Journal,* Vol. 21, Dec. 1983, pp. 1652-1666.

[18]Ericsson, L. E., "Karman Vortex Shedding and the Effect of Body Motion," *AIAA Journal,* Vol. 18, Aug. 1980, pp. 935-944.

[19]Beyers, M. E., "Direct Derivative Measurements in the Presence of Sting Plunging," AIAA Paper 84-2107, Aug. 1984 (see also *Journal of Aircraft,* Vol. 23, March 1986, pp. 179-185).